Supporting Information

Improving Near-Room-Temperature Thermoelectrics: The Role of Ag_2Se Doping and Bi/Sb Ratio in $(Bi, Sb)_2Te_3$

Wenxin Ou,[a#] Ruiheng Li,[a#] Chunliang Zhou,[b#] Yuange Luo,[a] Yin Xie,[a] and Ran Ang[a,c*]

[a]Key Laboratory of Radiation Physics and Technology, Ministry of Education, Institute of Nuclear Science and Technology, Sichuan University, Chengdu 610064, China

[b] Yantai Research Institute, Harbin Engineering University, Yantai 264006, China

[c]Institute of New Energy and Low-Carbon Technology, Sichuan University, Chengdu 610065, China

#Wenxin Ou, Ruiheng Li, and Chunliang Zhou contributed equally to this work.

*Corresponding author and Email: rang@scu.edu.cn

The single parabolic (SPB) model[1]

Within the SPB model, the transport parameters are expressed as follows:

$$S = \frac{k_B}{e}\left[\frac{2F_1}{F_0} - (\eta - \Delta)\right] \tag{S1}$$

Where k_B, e, F_0 and F_1, η, and Δ is respectively the Boltzmann constant, electron charge, Fermi integrals, the reduced chemical potential and the reduced energy difference between the bottoms of the two bands,

$$\Delta = E_V / k_B T \tag{S2}$$

The carrier concentration n_H:

$$n_H = 4\pi\left(\frac{2m^* k_B T}{h^2}\right)^{3/2} F_{1/2}(\eta - \Delta) \tag{S3}$$

Where m^* is the density of state effective mass taking into account band degeneracy, h is the Plank's constant, T is the absolute temperature. The mobility μ_H:

$$\mu_H = \mu_0 \frac{F_{-1/2}}{2F_0} = \frac{\tau_0 e F_{-1/2}}{m^* \ 2F_0} \tag{S4}$$

Where τ_0 is the relaxation time, which is closely related to the energy in the case of acoustic phonon scattering:[2]

$$\tau_0 = \frac{h^4 C_l}{8\sqrt{2}\pi^3 E_{def}{}^2 m^* k T^{3/2}} \tag{S5}$$

Where C_l is a parameter determined by the combination of the elastic constant,[3] and E_{def} is a combination of deformation potentials for multivalley systems. The Hall factor A is given by:

$$A = \frac{3}{2} F_{1/2}(\eta) \frac{F_{-1/2}}{2F_0^2} \tag{S6}$$

The Hall factor reflects the energy scattering mechanism and the anisotropy of the energy band. In the SPB model, anisotropy does not need to be considered. The Lorenz number L is defined as:

$$L = \frac{k_B{}^2 3F_0F_2 - 4F_1^2}{e^2 \qquad F_0^2} \tag{S7}$$

And the integral F_j above is defined by:

$$F_j(\eta) = \int_0^\infty \frac{\xi^j d\xi}{1 + e^{(\xi - \eta)}} \tag{S8}$$

Calculation of lattice thermal conductivity

The total relaxation time τ_{tot} can be calculated using Matthiessen's rule:[4]

$$\tau_{tot}^{-1} = \tau_{UN}^{-1} + \tau_{PD}^{-1} + \tau_{GB}^{-1} \tag{S9}$$

Where τ_{UN}, τ_{PD} and τ_{GB} correspond to the relaxation times for Umklapp-process scattering, point defect scattering, grain boundary scattering, and stacking fault scattering, respectively. The relevant phonon relaxation times are given by:

Umklapp phonon-phonon scattering:

$$\tau_{UN}^{-1} = A_N \frac{2 \quad k_B \bar{V}^{\frac{1}{3}} \gamma^2 \omega^2 T}{\left(6\pi^2\right)^{\frac{1}{3}} \quad \bar{M} v^3} \tag{S10}$$

Point defect phonon scattering:

$$\tau_{PD}^{-1} = \frac{\bar{V}\omega^4}{4\pi v^3}\Gamma \tag{S11}$$

Grain boundary phonon scattering:

$$\tau_{GB}^{-1} = \frac{v}{d} \tag{S12}$$

Where γ is the Grüneisen parameter, $\bar{M}$ is the average mass, m^* is the effective mass of charger carrier, ρ is the sample density, $\bar{V}$ is the average atomic volume, Γ is the point defect scattering parameter (which is determined by the mass difference), and d is the grain size. The Umklapp phonon–phonon scattering strength coefficient A_N is fit to the experimental data of the in-plane κ_l of fully dense samples.

Calculation of bipolar thermal conductivity

In *n*-type Bi_2Te_3-based materials around 303 K, acoustic phonon scattering is the dominant mechanism for carrier scattering. As a result, the electron mobility (μ_e) follows the relationship $\mu_e \sim T^{-3/2}$. As shown in Figure S6b, the calculated electron concentration (n_e) for all samples exhibits an empirical dependence of $n_e \sim T^{7.5}$. Therefore, the qualitative relationship between μ_e and n is derived as: $\mu_e \approx B n_e^{-1/5}$, where B is a temperature-independent constant for the fixed component (as shown in Table S1).

Supplementary details

Figure S1. (a,b) Grain size distribution of $Bi_{0.3}Sb_{1.7}Te_3$-*x* mol% Ag_2Se (*x* = 0, 0.1).

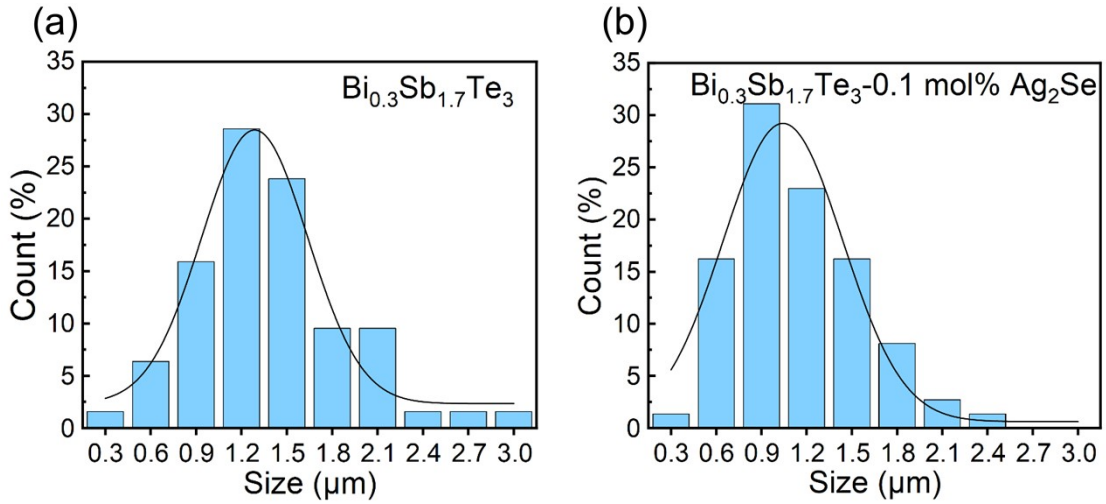

Figure S2. The Pisarenko plot of n_H-S for $Bi_{0.3}Sb_{1.7}Te_3$-x mol% Ag_2Se (x = 0, 0.05, 0.075, 0.1, 0.125) and $Bi_ySb_{2-y}Te_3$-0.1 mol% Ag_2Se (y = 0.3, 0.4, 0.5, 0.6) samples at 303 K.

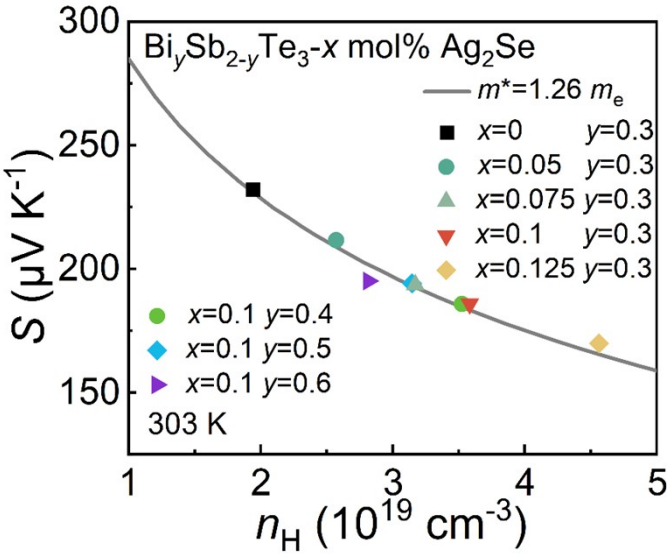

Figure S3. (a) Electrical thermal conductivity (κ_e) of $Bi_{0.3}Sb_{1.7}Te_3$-x mol% Ag_2Se and (b) κ_e of $Bi_ySb_{2-y}Te_3$-0.1 mol% Ag_2Se samples.

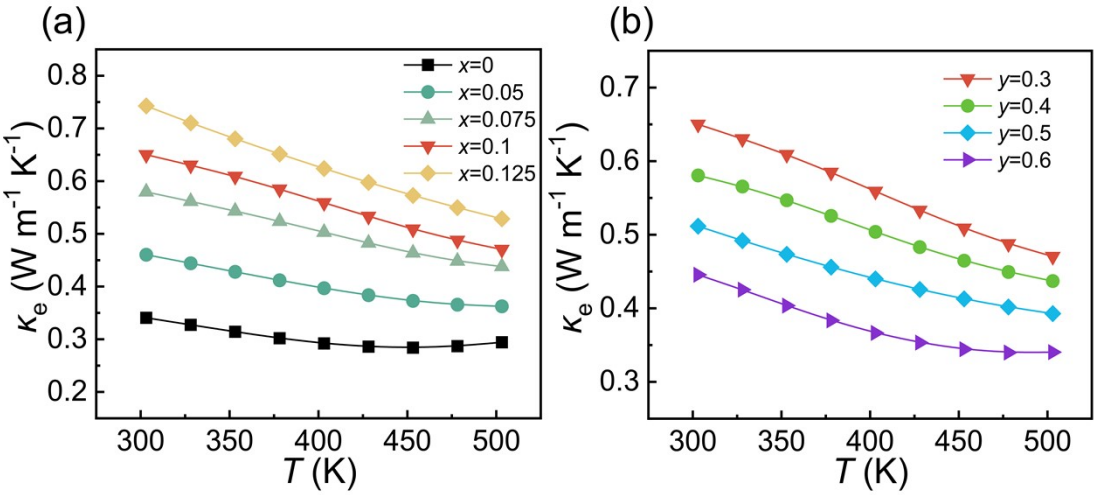

Figure S4. Temperature dependence of the calculated (a) carrier concentration (n_H) and (b) electron concentration (n_e) for the $Bi_{0.3}Sb_{1.7}Te_3$-x mol% Ag_2Se samples.

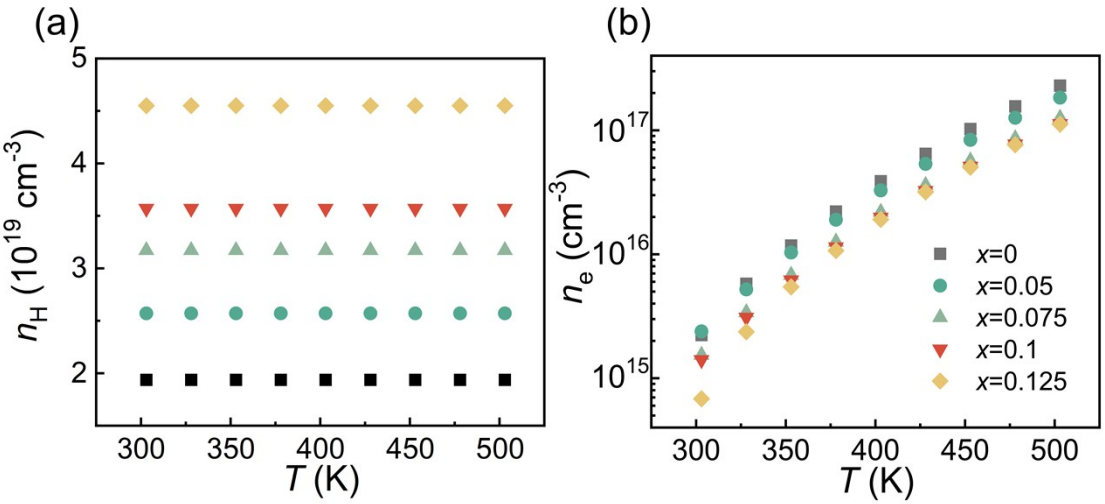

Figure S5. Variation of carrier concentration (n_H) and mobility (μ_H) with y content in $Bi_ySb_{2-y}Te_3$-0.1 mol% Ag_2Se at 303 K.

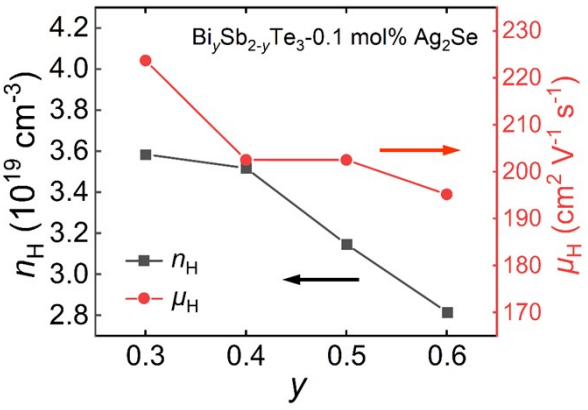

Figure S6. Temperature-dependent (a) electrical conductivity (σ); (b) Seebeck coefficient (S); (c) power factor (PF); (d) total thermal conductivity (κ_t); (e) lattice plus bipolar thermal conductivity ($\kappa_l + \kappa_b$); (f) figure of merit (zT) for $Bi_{0.4}Sb_{1.6}Te_3$-0.1 mol%Ag_2Se sample tested perpendicular (in-plane) and parallel (out-of-plane) to the uniaxial high-voltage direction.

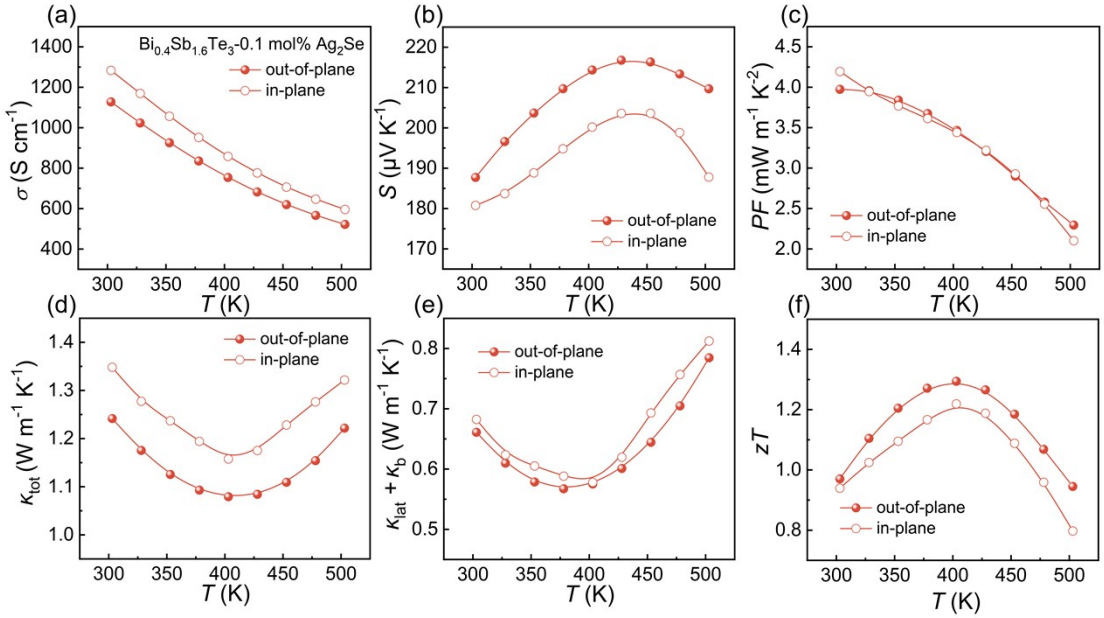

Figure S7. TE devices made of commercially available *n*-type $Bi_2Te_{2.7}Se_{0.3}$ and *p*-type $Bi_{0.5}Sb_{1.5}Te_3$ (a) Output voltage (U); (b) Output power (P); (c) Heat flow (Q); (d) Conversion efficiency (η) as a function of current (I).

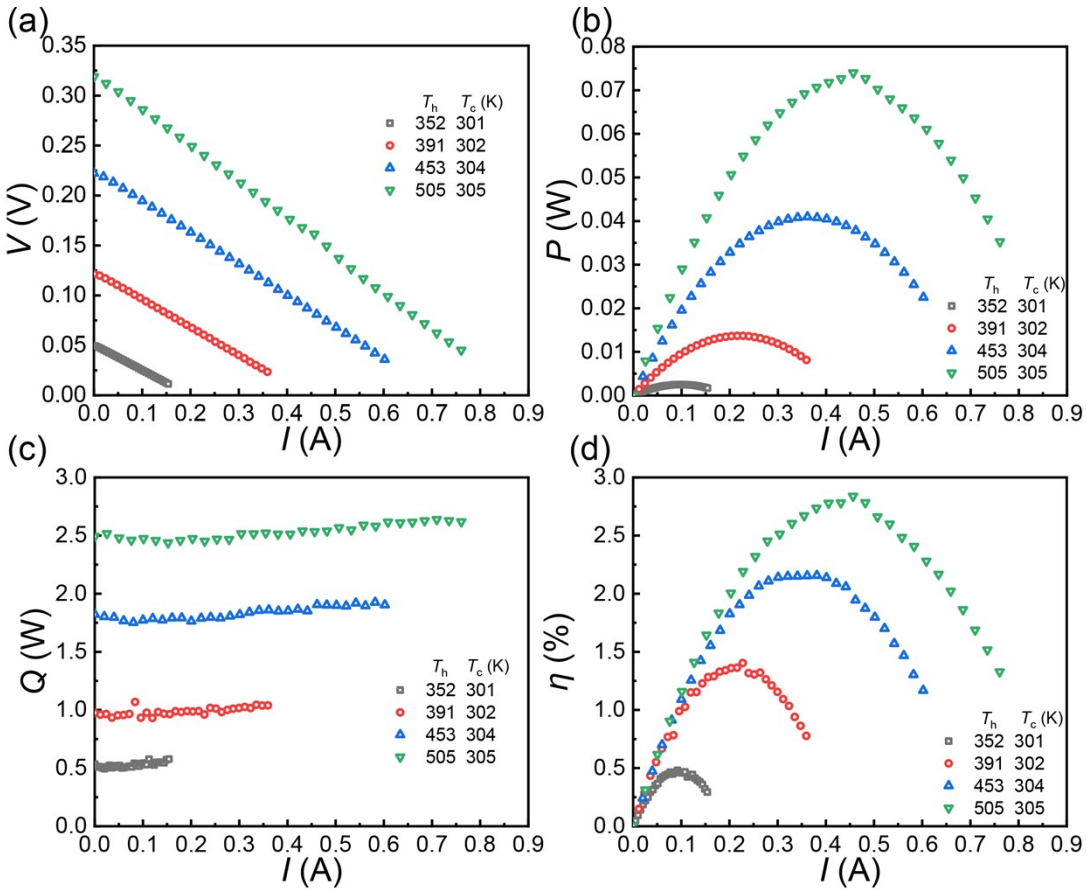

Supplementary Tables

Table S1. Calculated parameters *A* and *B* using the minor and major carrier concentrations at 303 K.

$Bi_{0.3}Sb_{1.7}Te_3$-*x* mol% Ag_2Se	*x* = 0	*x* = 0.05	*x* = 0.075	*x* = 0.1	*x* = 0.125
$A(10^{30}cm^{-6})$	3.24	2.72	2.49	2.45	2.33
B	1.58	1.37	1.68	1.55	1.22

Table S2. Parameters used for the calculation of lattice thermal conductivity.

Parameters	Description	Values	Ref.
θ_D	Debye temperature	124	5
γ	Grüneisen parameter	2.3	5
r	Poisson's ratio	0.25	5
v_L	Longitudinal sound velocity	2988 m·s^{-1}	5
v_T	Transverse sound velocity	1721 m·s^{-1}	5
Γ	Point defect scattering parameter	0.175	5
v	Average speed of sound	2147 m·s^{-1}	6
$\bar{V}$	Average atomic volume of $Bi_{0.3}Sb_{1.7}Te_3$	3.13×10^{-29} m^3	6
$V_{Bi_2Te_3}$	Atomic volume of Bi_2Te_3	3.40×10^{-29} m^3	6
$V_{Sb_2Te_3}$	Atomic volume of Sb_2Te_3	3.31×10^{-29} m^3	6
$M_{Bi_2Te_3}$	Average atomic mass of Bi_2Te_3	2.79×10^{-25} kg	7
$M_{Sb_2Te_3}$	Average atomic mass of Sb_2Te_3	2.07×10^{-25} kg	7
A_N	Comprehensive coefficient between Umklapp and Normal processes	2.3	fitted
$\bar{M}$	Average atomic mass of $Bi_{0.3}Sb_{1.7}Te_3$	2.2×10^{-25} kg	fitted
d	Grain size	1.2	Exp.

Table S3. Relevant parameters of commercially available *n*-type $Bi_2Te_{2.7}Se_{0.3}$ and *p*-type $Bi_{0.5}Sb_{1.5}Te_{3.}$

Project	Technical requirement	Unit	Remark
Product model	*n*-type crystal rod	/	
Production technology	zone melting pulling crystals	/	
Seebeck coefficient	≤-200	μV K^{-1}	Test temperature 300K
Electric conductivity	1000±5%	S cm^{-1}	Test temperature 300K
Thermal conductivity	1.42±5%	W m^{-1} K^{-1}	Test temperature 300K
zT	0.86	/	Test temperature 300K
Compressive strength	35±5	MPa	
Product model	*p*-type-SPS900	/	
Production technology	powder metallurgy	/	
Seebeck coefficient	≥200	μV K^{-1}	Test temperature 300K
Electric conductivity	1000±10%	S cm^{-1}	Test temperature 300K
Thermal conductivity	1.35±5%	W m^{-1} K^{-1}	Test temperature 300K
zT	0.95	/	Test temperature 300K
Compressive strength	65±5	MPa	

Notes and references

1 M. Zhou, Z. M. Gibbs, H. Wang, Y. Han, C. Xin, L. Li and G. J. Snyder, *Phys. Chem. Chem. Phys.*, 2014, **16**, 20741–20748.

2 Y. Xiao, H. Wu, W. Li, M. Yin, Y. Pei, Y. Zhang, L. Fu, Y. Chen, S. J. Pennycook, L. Huang, J. He and L.-D. Zhao, *J. Am. Chem. Soc.*, 2017, **139**, 18732–18738.

3 C. Herring and E. Vogt, *Phys. Rev.*, 1956, **101**, 944–961.

4 T. J. Zhu, C. G. Fu, H. H. Xie, Y. T. Liu, B. Feng, J. Xie and X. B. Zhao, *Epl-Europhys Lett.*, 2013, **104**, 46003.

5 H.-L. Zhuang, H. Hu, J. Pei, B. Su, J.-W. Li, Y. Jiang, Z. Han and J.-F. Li, *Energy Environ. Sci.*, 2022, **15**, 2039–2048.

6 Q. Zhang, M. Yuan, K. Pang, Y. Zhang, R. Wang, X. Tan, G. Wu, H. Hu, J. Wu, P. Sun, G.-Q. Liu and J. Jiang, *Adv. Mater.*, 2023, **35**, 2300338.

7 S. I. Kim, K. H. Lee, H. A. Mun, H. S. Kim, S. W. Hwang, J. W. Roh, D. J. Yang, W. H. Shin, X. S. Li, Y. H. Lee, G. J. Snyder and S. W. Kim, *Science*, 2015, **348**, 109-114.